Structure and dynamics of NiAl(110) studied by high-resolution ion scattering combined with density functional calculations

Tetsuya Kogita,[1] Masanori Kohyama,[2] and Yoshiaki Kido[1,*]
[1]*Department of Physics, Ritsumeikan University, Kusatsu, Shiga-ken 525-8577, Japan*
[2]*Advanced Industrial Science and Technology (AIST), Ikeda, Osaka 563-8577, Japan*
(Received 28 April 2009; revised manuscript received 13 October 2009; published 9 December 2009)

The surface relaxation and the rumpling of the top layer and the second layer together with the mean thermal vibration amplitudes of NiAl(110) are determined by high-resolution medium energy ion scattering (MEIS) with an excellent depth resolution of typically ± 0.01 Å. We also perform classical molecular-dynamics (MD) simulations employing the embedded atom method and the first-principles calculations using the VASP (Vienna *ab initio* simulation package) code. The results obtained by MEIS are compared with the theoretical predictions and experimental analysis reported so far. Interestingly, the present MEIS analysis observes slightly expanded relaxation $\Delta\varepsilon_{12}$, which is supported by the present MD and VASP calculations and by x-ray diffraction analysis whereas other experimental and theoretical analyses give contracted relaxation. The root-mean-square thermal vibration amplitude of the bulk Ni atoms is determined to be 0.10 ± 0.005 Å, which agrees well with the value of 0.097 Å derived from the phonon-dispersion relation calculated from VASP. A slightly enhanced thermal vibration amplitude of the top-layer Ni in the surface-normal direction observed is consistent with the MD simulation.

DOI: 10.1103/PhysRevB.80.235414 PACS number(s): 68.35.bd, 68.35.Md, 68.47.De, 68.49.Sf

I. INTRODUCTION

In a previous study,[1] we analyzed the surface relaxation and thermal vibration amplitudes (TVAs) of Cu(111) and Ni(111) by high-resolution medium energy ion scattering (MEIS). The results obtained by MEIS are in good agreement with the molecular-dynamics (MD) simulations using the embedded atom method (EAM). One of the aims to pursue the present analysis is to test the classical MD using EAM potentials applied to a binary-alloy system. It is also interesting to compare the experimental results with the first-principles calculations.[2,3] Nickel aluminum with CsCl structure is a representative intermetallic compound and many investigations using various kinds of experimental and theoretical techniques reported considerably large rumpling of the top layer of NiAl(110),[4–11] quite similar to alkali-halide surfaces. In addition, NiAl(110) has such an attractive nature that on the surface-ordered aluminum-oxide layers[12–15] grow, which are free from charge up by photon, electron, and ion irradiations and thus are frequently utilized as a support of metal clusters.[16–19]

In this study, we determine the top-layer and second-layer rumpling and the interplanar distances of the top and second Ni and Al planes by high-resolution MEIS with an excellent height resolution of typically ± 0.01 Å. The bulk and enhanced TVAs of Ni atoms are also determined. The clean NiAl(110)-1×1 surface was prepared by sputtering-annealing cycles and confirmed by MEIS and reflection high-energy diffraction (RHEED). Immediately after the surface cleaning, the sample was transferred to a scattering chamber for MEIS without exposure to air. The results obtained by MEIS are compared with our MD simulations using EAM potentials and the first-principles calculations using the VASP (Vienna *ab initio* simulation package) codes.

II. EXPERIMENT

We employed the NiAl(110) crystals with a diameter of 11 mm and thickness of 2 mm which was purchased from Surface Preparation Laboratory (SPL) in the Netherlands. The surface was sputtered with 1.5 keV Ar^+ for 20 min and then annealed in ultrahigh vacuum (UHV) at 1030 °C for 20 min. We repeated this cycle two times and then observed a clean 1×1 pattern by RHEED using 25 keV electron beams. No surface contaminations such as C and O (below 1×10^{13} atoms/cm^2; <0.6 at. %) were detected by MEIS. In the present MEIS analysis we used 120 keV He^+ ions, which were collimated to a size of 0.17 mm in horizontal and 2.0 mm in vertical planes. The small horizontal and relatively large vertical sizes give an excellent energy resolution and statistics, respectively. Samples were mounted on a six-axis goniometer, three axis for rotation and three axis for translation. Scattered He^+ ions were detected by a toroidal electrostatic analyzer fixed on a turn table giving an excellent energy resolution of $\Delta E/E=1.0\times10^{-3}$. In our MEIS system, a central circular trajectory for deflected ions was set in a horizontal plane and an applied voltage was fixed during data acquisition. Note that our toroidal spectrometer has a large interelectrode distance of 16 mm, which covers 10% of a pass energy at a fixed applied voltage. Deflected ions were imaged on a three-stage microchannel plate combined with a position sensitive detector of a semiconductor type (MCP/PSD) with a spatial resolution of 40 μm. The details of the MEIS system were described elsewhere.[20–22]

Figure 1 shows a typical MEIS spectrum taken for 119.84 keV He^+ ions incident along the $[\bar{1}01]$ axis and scattered to the $[10\bar{1}]$ direction. This spectrum was obtained by connecting two MEIS spectra, (i) higher-energy part (Ni) and (ii) lower-energy part (Al). A steplike feature seen around 104.5 keV [corresponding to a border of (i) and (ii)] is caused mainly by a degraded detection efficiency near the edge of

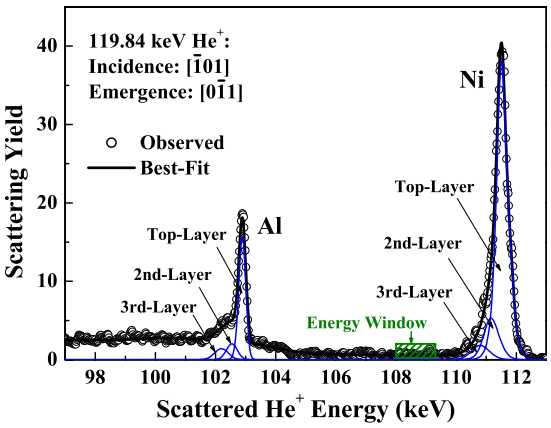

FIG. 1. (Color online) Typical MEIS spectrum observed for 120 keV He^+ ions incident along [$\bar{1}$01] axis and scattered to [0$\bar{1}$1] direction. Solid curves are the best-fitted spectra involving total (thick) and deconvoluted (thin) spectra (scattering components from first, second, and third layers).

the MCP/PSD. The observed MEIS spectrum is best fitted assuming appropriate hitting and blocking probabilities for the second-layer and third-layer Ni and Al atoms. Here, the hitting probability for the top-layer atoms is normalized to unity (no shadowing) and an exponentially modified Gaussian shape[23,24] is employed for the scattering component from each atomic layer. Stoichiometric Ni/Al ratio in the top layer is estimated from the ratio of the scattering yield from Ni to that from Al considering a nonequilibrium charge fractions[25] of He^+ and assuming correct chemical ordering. To confirm the stoichiometry and correct chemical ordering in the underlying layers from MEIS spectra is difficult because of many fitting parameters such as enhanced and correlated thermal vibration amplitudes. In order to avoid surface damage induced by ion irradiation and buildup of surface contamination such as oxide, we shifted slightly the beam position on the sample surface after irradiation of 1 μC and cleaned again the surface after 5–6 hours working. All the experiments were carried out *in situ* under UHV conditions ($\leq 2 \times 10^{-10}$ Torr) at Beamline 8 named SORIS at Ritsumeikan SR Center.

III. MD SIMULATIONS AND FIRST-PRINCIPLES CALCULATIONS

A. MD simulation

The MD simulations using the EAM potentials[26,27] were successfully applied to the surface relaxation and enhanced and correlated TVAs of Ni(111) and Cu(111) crystals.[1] The idea of the EAM is to introduce the density functional treatment[28] and to approximate the electron density at a position near a lattice site by linear superposition of valence electrons of neighboring atoms. It is interesting to perform the MD simulations using EAM potentials for a typical binary alloy of NiAl(110) and to compare the results with experimental data derived from MEIS analysis. The MD simulations using EAM were already carried out to study the martensitic phase transition in Ni_xAl_{1-x} (Ref. 29) and the planar faults and point-defect characteristics of B2 NiAl.[30]

According to Daw and Baskes,[26] the total energy of each composite atom i of a solid can be approximated by

$$E_i(\vec{R}_i) = F_i[\rho_i(\vec{R}_i)] + \frac{1}{2}\sum_{j\neq i}\phi_{ij}(R_{ij}), \tag{1}$$

where

$$\rho_i(\vec{R}_i) = \sum_{j\neq i}\rho_j(R_{ij}). \tag{2}$$

The first term, $F_i[\rho_i(\vec{R}_i)]$ in Eq. (1) is the energy gained by embedding atom i into the position $\vec{R}_i$ surrounded by the background electron density $\rho_i(\vec{R}_i)$ and the second term corresponds to the repulsive interaction between the positive core of atom i and another positive core j. The background electron density consists of $3d(n_d)$ and $4s(n_s)$ electrons from Ni and of $2p(n_p)$ and $3s(n_s)$ electrons from Al and is expressed by

$$\rho_i(\vec{R}_i) = \sum_{j\neq i}\{n_s\rho_{sj}^{\mathrm{Ni}}(R_{ij}) + n_d\rho_{dj}^{\mathrm{Ni}}(R_{ij})\} + \sum_{k\neq i}\{n_s\rho_{sk}^{\mathrm{Al}}(R_{ij}) + n_p\rho_{pk}^{\mathrm{Al}}(R_{ij})\}, \tag{3}$$

where $\rho_{\sigma j}(R_{ij})$ is the electron density of σ (s,p,d) shell provided by atom j at a position $\vec{R}_i$, and R_{ij} is the internuclear distance between atoms i and j. The electron density is calculated from the Hartree-Fock-Slater atomic model.[31] The repulsive interaction between positive cores i and j are given by

$$\phi_{ij}(R_{ij}) = \frac{Z_i(R_{ij})Z_j(R_{ij})}{R_{ij}}, \tag{4}$$

where

$$Z_i(R) = Z_a(1+\beta R^{\nu})e^{-\alpha R}. \tag{5}$$

The above fitting parameters (Z_a,β,ν,α) are given to reproduce the experimental values such as cohesive energy, bulk modulus, and elastic constants of NiAl. We adopted the fitting parameters proposed by Rubini and Ballone,[29] which reproduce well the martensitic phase-transformation temperatures.

In the present MD simulations (microcanonical ensemble), we set a basic cell comprising $16\times16=256$ atoms in the (x,y) plane (x axis: [001] and y axis: [1$\bar{1}$0]) and 16 atomic layers in the z direction [110]. The basic cell is surrounded by eight image cells placed in the (x,y) plane and satisfying boundary conditions and as a result the system takes a rectangular cell of $48\times48=2304$ atoms in the (x,y) plane and a height of 16 atomic layers. We calculated the total energy of the system by varying the lattice constant, which takes a minimum value at a lattice constant a of 2.8882 Å for a cutoff radius above 8.0 Å. This is quite consistent with the value of 2.887 Å given by x-ray diffraction[32] and with $a=2.88$ Å tabulated in the textbook of Kittel.[33] We solve the equation of motion, $\vec{f}_i(\vec{R}_i)=-\nabla_i E_i(\rho(\vec{R}_i)$ by the Verlet method at a time interval of 5.0 fs. A thermal equilibrium was maintained after a time lapse of ~10 ps with a

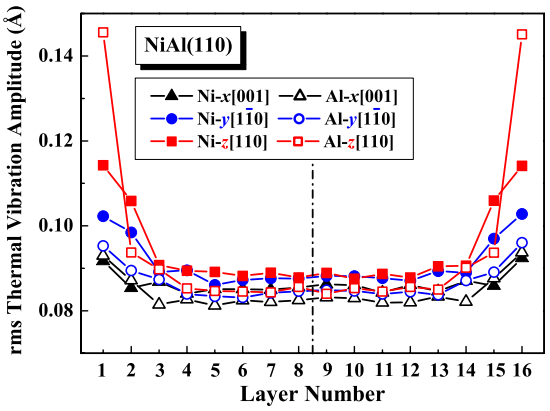

FIG. 2. (Color online) Root-mean-square thermal vibration amplitudes as a function of layer number calculated by MD simulations for Al (open) and Ni (closed) atoms along the [110] (squares), [1$\bar{1}$0] (circles), and [001] (triangles) directions.

velocity distribution coinciding with the Maxwell distribution and the temperature was set to 300 K with a fluctuation of ±5%. Increases in the number of atoms in the basic cell reduces the fluctuation. Another check point in the MD simulations is the velocity of center of mass, which is intentionally fixed to 0 cm/s, as an initial condition and confirmed to be below 10^{-8} cm/s after the arrangement. After confirming a thermal equilibrium, we calculated the positions of Al and Ni in each atomic layer by time averaging over a period of 200 fs with sampling times of 10.

The interplanar distances between top and second Ni planes and between top and second Al planes are derived to be 1.94 and 2.36 Å, respectively, and the top Al plane is expanded toward the vacuum side by 0.25 Å relative to the top Ni plane. Thus the relaxation $\Delta\varepsilon_{12}$ results in +0.11 Å and the rumpling of the second layer is determined to be −0.17 Å, respectively. Here, the relaxation $\Delta\varepsilon_{12}$ and rumpling $\Delta\varepsilon(n)$ in the nth layer are defined by

$$\Delta\varepsilon_{12} = \frac{(h_{\mathrm{Al}}^{(1)} + h_{\mathrm{Ni}}^{(1)}) - (h_{\mathrm{Al}}^{(2)} + h_{\mathrm{Ni}}^{(2)})}{2} - d_{bulk} = \varepsilon_{12} - d_{bulk},$$

$$\Delta\varepsilon(n) = h_{\mathrm{Al}}^{(n)} - h_{\mathrm{Ni}}^{(n)}, \tag{6}$$

where $h_{\mathrm{Al}}^{(n)}$ and d_{bulk} are the height of the nth Al plane and the bulk interlayer distance of the NiAl(110) layer.

We also determine enhanced and correlated TVAs together with the bulk TVAs for Ni and Al atoms at 300 K. Figure 2 shows the root-mean-square (rms) TVAs of Ni and Al atoms in the nth layer ($n=1,\ldots,16$) along the x-([001]), y-([1$\bar{1}$0]), and z-([110]) directions. Here, the layer number 1 and 16 correspond to the top layer (top surface). As pointed out previously,[34] long-period oscillations appear in the (x,y) plane, which are caused by the fixed boundary for the (x,y) plane and free boundary for the surface-normal direction (z axis). The effect of this apparent oscillatory behavior can be avoided by averaging rms TVAs in the (x,y) plane over a relatively short-time lapse ($\sim 2\times 10^{-13}$ s). As expected, the TVAs of the top-layer Ni and Al atoms, in particular, Al atoms are strongly enhanced in the surface-normal direction (z axis). This is due to the fact that the top Al plane is expanded toward the vacuum side by 0.25 Å relative to the top Ni plane. However, the TVAs of Al and Ni atoms in deeper layers below the third layer are almost constant and thus the one-dimensional (1D) TVAs for bulk Al and Ni are estimated to be 0.084 ± 0.003 and 0.087 ± 0.003 Å, respectively. Interestingly, the TVA of Ni with a mass almost twice the Al mass is slightly larger than that of Al. The results obtained by the MD simulations are indicated in Table I.

B. First-principles calculations

The static surface structure for NiAl(110) and phonon-dispersion relation of bulk NiAl are calculated using the VASP codes[2,3] in a plane-wave supercell approach. The slab unit cell for calculating the (110) surface structure consists of $1\times1(x,y)\times9(z)$ atoms and the atoms in the first five layers can be displaced but another four layers are fixed. To construct the three-dimensional (3D) periodicity, nine vacant layers (~24 Å) are inserted between the slabs along the [110] axis (z direction). We employ the Perdew-Burke-Ernzerhof-type generalized gradient approximation for exchange-correlation energy[35] and use the projector-augmented wave (PAW) method as the pseudopotential scheme.[36] The cutoff energy for the plane-wave basis is set to 350 eV and the $\vec{k}$-point sampling of $25\times25\times3$ is reduced to 455 points in the irreducible part of the first Brillouin zone (BZ). We adopt the RMM-DIIS (residual minimization/direct inversion in the iterative subspace) algorithm[37] for efficient electronic minimization. Note that NiAl is a nonmagnetic metal with a filled d band and thus there is no need to perform spin-polarized calculations. The results obtained for the surface relaxation and rumpling are indicated in Table I.

We also calculate the phonon-dispersion relation for the NiAl(110) bulk, which is obtained by solving the equations of motion for Al and Ni atoms located on the lattice sites assuming $45\times45\times45$ $\vec{q}$ points in the first Brillouin zone. The force constants are derived from the Hellmann-Feynman force calculated by displacing the atoms by 0.1% of the lattice constant from the equilibrium lattice-site positions in the supercell containing $2\times(3\times3\times3)=54$ atoms. In this calculations, the cutoff energy is set to 400 eV and $9\times9\times9$ $\vec{k}$-points mesh reduced to 75 points are used to integrate over the first BZ of the supercell and the conjugate gradient method[37,38] is adopted for the electronic minimization. We sought solutions to the equation of motion in the form of plane waves satisfying the Bloch condition. This leads to a six-order secular equation for phonon frequencies $\omega_\lambda(\vec{q})$ corresponding to six linear simultaneous equations, which were solved numerically. Figure 3 shows the phonon-dispersion relations for the bulk NiAl, which are compared with experimental data measured by neutron scattering.[39] It is clearly seen that the result obtained here is in good agreement with the experimental data. The expectation value of the scalar product of displacement vectors $\vec{u}$ for atoms taking lattice positions $\vec{l}$ and $(\vec{l}+n\vec{d})$ is calculated from the dispersion relation $\omega_\lambda(\vec{q})$ ($\lambda=1,\ldots,6$: phonon modes, such as transverse optical and acoustic modes),[40,41]

TABLE I. Surface relaxation ($\Delta\varepsilon_{12}$) and rumpling $[\Delta\varepsilon(1), \Delta\varepsilon(2)]$ and rms 1D TVAs of Ni of bulk NiAl (σ_{Ni}) and top-layer Ni in the surface-normal direction $[\sigma_{\perp}^{\mathrm{Ni}}(1)]$. Present MEIS results are compared with MD and VASP calculations and with experimental and theoretical predictions reported previously.

	$\Delta\varepsilon_{12}$ (Å)	$\Delta\varepsilon(1)$ (Å)	$\Delta\varepsilon(2)$ (Å)	σ_{Ni} (Å)	$\sigma_{\perp}^{\mathrm{Ni}}(1)$ (Å)
Present MEIS	$+0.06 \pm 0.02$	$+0.12 \pm 0.02$	-0.11 ± 0.03	0.10 ± 0.005	0.105 ± 0.01
Present MD	+0.11	+0.25	−0.17	0.087 ± 0.004	0.114 ± 0.003
Present VASP	+0.01	+0.17	$+0.04 \pm 0.05$	0.097	
Yalisove (MEIS)[a]	-0.02 ± 0.04	$+0.20 \pm 0.04$	-0.04 ± 0.08		
XRD[b]	$+0.01 \pm 0.01$	$+0.16 \pm 0.01$	-0.01 ± 0.01	0.08	
LEED[c]	-0.03 ± 0.04	$+0.22 \pm 0.04$	0		
FLAPW[d]	−0.13	+0.20	0		
PWPP[e]	−0.05	+0.23	0		
Rivière (VASP)[f]	+0.07	+0.17	-0.03 ± 0.05		
Mishin (MD)[g]	−0.08	+0.14	−0.18		

[a]Reference 5.
[b]Reference 7.
[c]Reference 11.
[d]Reference 8.
[e]Reference 9.
[f]Reference 10.
[g]Reference 30.

$$\langle\Phi|\vec{u}(\vec{l};j)\cdot\vec{u}(\vec{l}+n\vec{d};k)|\Phi\rangle = \frac{\hbar}{\sqrt{M_j M_k}\Omega_{\mathrm{BZ}}}\int\sum_{\lambda}\frac{1}{\omega_{\lambda}(\vec{q})} \times\left[\frac{1}{\exp\{\omega_{\lambda}(\vec{q})\hbar/k_B T\}-1}+\frac{1}{2}\right] \times\cos(\vec{q}\cdot n\vec{d})d\vec{q}, \quad (7)$$

where $|\Phi\rangle$, M_j (M_k), and Ω_{BZ} are the eigenfunction of phonon field, atomic mass (Al or Ni), and the volume of the first Brillouin zone, respectively. Here, T denotes an absolute temperature, and $\hbar$ and k_B are the Planck and Boltzmann constants. This expression gives the correlated TVA between the nth nearest-neighbor atoms. If one puts $n=0$, the square of rms (3D) TVA of the bulk j atoms is obtained.

IV. MEIS ANALYSIS

The details how to analyze the NiAl(110) surface by MEIS is presented in the literature.[15] The stopping powers of Ni and Al together with the He^+ fractions dependent upon emerging energy and angle were determined in advance and the Lindhard-Scharff formula[42] is used as energy straggling. We performed angular scans around (i) $[\bar{1}\bar{1}3]$, (ii) $[\bar{3}11]$, and (iii) $[\bar{1}01]$ axis at a fixed emerging angle (random direction). The above scattering geometries determine the interplanar distance (i) between top Ni and second Al planes, (ii) between top Al and second Ni planes, and (iii) between top and second Ni planes. Figures 4(a)–4(c) show the angular scans for scattering components from the second-layer Al, Ni, and Ni atoms (open circles), respectively, and from deeper-layers Ni atoms (open triangles). Here, the observed scattering yield is divided by the corresponding scattering cross section because the scattering angle was varied in the angular scan. From the angular shifts giving minimum scattering yields, as shown in the figures, we can determine the interplanar distances mentioned above from a simple trigonometry.[43] The scattering yield from the second-layer atoms as a function of incident angle is least-square fitted (dotted curves) with polynomials. The rumpling of the top and sercond layers together with the relaxation (interlayer distance between the top and second layer: ε_{12}) is shown in Fig. 5, schematically. Here, we assumed the lattice constant of 2.887 Å, which was determined by x-ray diffraction analysis.[32] The surface is terminated with the Al plane displaced toward the vacuum side by 0.12 Å from the top Ni plane. In contrast, in the second layer, the Ni plane is located toward the upward direction by 0.11 Å relative to the second Al plane. Concerning the rumpling of the top and second layers, the present result is compatible with that determined by MEIS previously.[5] However, the present MEIS analysis shows a significant expansion of the first interlayer distance, which is opposed to the previous MEIS result[5] (see Table I). It must be noted here that the

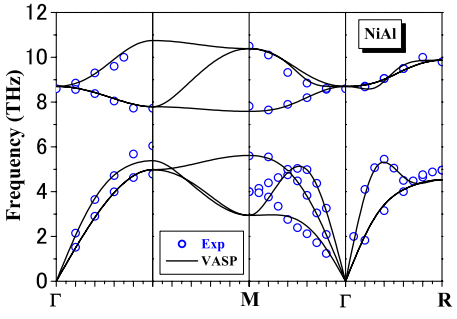

FIG. 3. (Color online) Phonon-dispersion relation for bulk NiAl calculated using VASP code. Open circles denote experimental data measured by neutron scattering (Ref. 39).

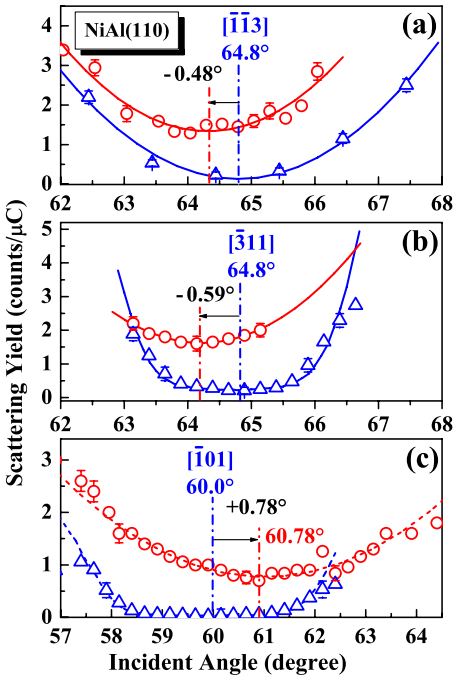

FIG. 4. (Color online) Angular scan spectra around (a) $[\bar{1}\bar{1}3]$, (b) $[\bar{3}11]$, and (c) $[\bar{1}01]$ axis for scattering components from the second (circles) and deeper layers (triangles) as a function of incident angle (emerging angle was fixed to random direction). Here, (a) second-layer Al is shadowed by top-layer Ni, (b) second-layer Ni is shadowed by top-layer Al, and (c) second-layer Ni is shadowed by top-layer Ni.

energy resolution of our MEIS system ($\Delta E/E \leq 1 \times 10^{-3}$) is better than the previous MEIS (Ref. 5) by a factor of 4.

Angular scan profiles for the scattering components from deeper layers are sensitive to the bulk TVAs and insensitive to enhanced TVAs of surface atoms and correlated thermal vibrations,[1,22,43] which was confirmed by Monte Carlo simulations of ion trajectories. Figure 6 shows the angular scan spectrum around the [100] axis in the (001) plane for 120 keV He^+ ions scattered primarily from fifth–tenth layers Ni atoms (see, for example, Fig. 1). The emerging angle was fixed to a random direction and the incident angle of 45.0° giving a minimum yield corresponds to the [100] axis with respect the surface normal. The solid curves in Fig. 6 are the hitting probabilities calculated from He^+ ion trajectories assuming 1D TVA (σ) of 0.08, 0.09, 0.10, 0.11, and 0.12 Å. Here, we assumed isotropic lattice vibrations because the polar scan profiles for the scattering components from deeper layers do not depend significantly on the correlated and enhanced TVAs.[44] It is clearly seen that assumption of $\sigma = 0.10$ Å gives the best fit to the observed profile. We also estimate the enhanced TVA of the top-layer Ni atoms to be 0.105 ± 0.005 Å in the surface-normal direction, which is derived from the close encounter probability of 0.35 ± 0.03 for the second-layer Ni atoms for 120 keV He^+ ions incident along the $[0\bar{1}\bar{1}]$ axis (the spectrum is not shown here). Such a relatively small enhancement may be due to neglecting the positive correlation (~+0.1) between the top and second-layer Ni atoms in the above analysis, which increases the TVA by several %.

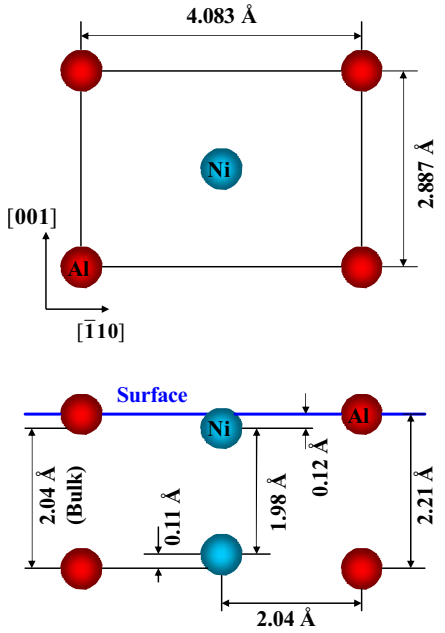

FIG. 5. (Color online) Schematic of top (upper) and side (lower) views of NiAl(110) surface (circles denote Al and Ni atoms). The interplanar distances indicated are determined by the present MEIS analysis.

V. RESULTS AND DISCUSSIONS

There are many reports on experimental and theoretical investigations of the surface relaxation and rumpling of NiAl(110). Concerning the rumpling of the top layer, all the analyses result in considerable outward displacement of Al and inward relaxation of Ni atoms (see Table I). In contrast, the Al atoms are displaced inward relative to the Ni atoms in the second layer. Only present VASP calculation predicts a slightly opposite rumpling for the second layer. Rivière *et al.*[10] performed minimizing the total energy using the VASP codes to give the rumpled NiAl(110) surface and obtained

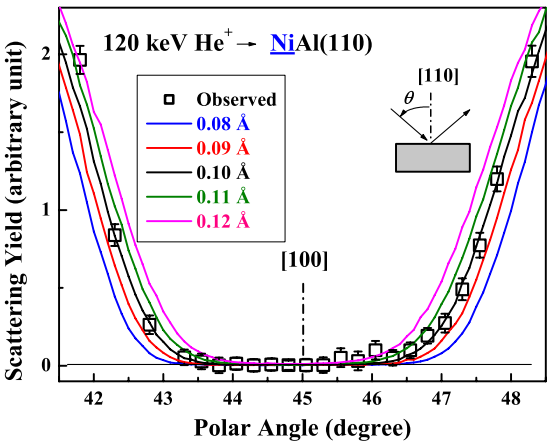

FIG. 6. (Color online) Hitting probabilities for 120 keV He^+ ions incident around [100] axis and scattered from Ni atoms primarily in fifth–tenth layers. Solid curves are calculated hitting probabilities assuming 1D TVA of 0.08, 0.09, 0.10, 0.11, and 0.12 Å for Ni atoms.

the lattice constant of 2.892 Å, which is compatible with our calculation also using the VASP by converging the lattice compressibility. However, it is quite delicate to determine the second-layer rumpling by minimizing the total energy because the energy difference of ~1 meV/atom changes significantly the relative height of Al and Ni planes in the second layer. It must be noted that practical surface structures are constructed by following not only energetics but also kinetics. The structure minimizing a total energy may or may not lead to a practical surface structure because the kinetics may play an important role in phase formation during surface treatments (atmospheres, temperature, heating and cooling time, sputtering, etc.). The present MEIS analysis shows a slight positive relaxation (expansion) for ε_{12}, which is also predicted by the present MD and VASP calculations and by the grazing-incidence XRD analysis using intense synchrotron-radiation source[7] while previous MEIS,[5] LEED,[11] and the *ab initio* calculations [FLAPW (Ref. 8): full-potential linearized augmented plane wave and PWPP (Ref. 9): plane-wave pseudopotential method) give contracted interlayer distances. The difference between the present MD and VASP results on the rumpling and relaxation is due to different temperatures (MD: 300 K and VASP: 0 K) and to different interaction potentials. The MD simulations using the EAM potential carried out by Mishin *et al.*[30] also give a negative relaxation (contraction), which is opposed to our MD simulations. This is due to different fitting parameters employed for the EAM potentials. Indeed, the lattice constant of 2.86 Å (Ref. 29) is significantly smaller than our value of 2.888 Å. It is important to test the parameters of EAM potentials by calculating mechanical properties such as elastic constants and lattice dynamics.

One dimensional TVA for the bulk Ni atoms derived from MEIS coincides well with that estimated from the phonon-dispersion relation which is calculated using the VASP codes (see Table I). The present MD and XRD analyses[7] give significantly smaller values. In the MD simulation scheme applied to a binary alloy, NiAl, for example, the embedded potential functions for Al and Ni are independently given to reproduce the cohesive energies of Al and Ni crystals. This seems problematic in applying the EAM to intermetallic alloys. In spite of this deficiency, the MD simulations give almost reasonable values on the surface structure and lattice dynamics. It is interesting to see the TVA for the bulk Al compared with that for the bulk Ni. According to the present MD simulation, the 1D TVA for the bulk Al is compatible with that for Ni ($\sigma_{\mathrm{Al}}=0.084\pm0.003$ and $\sigma_{\mathrm{Ni}}=0.087\pm0.003$ Å) while the VASP calculation gives much larger TVA for Al than that for Ni ($\sigma_{\mathrm{Al}}=0.142$ and $\sigma_{\mathrm{Ni}}=0.097$ Å) according to Eq. (7). Unfortunately, in the MEIS analysis, it is difficult to determine the σ_{Al} value because of a small scattering yield from Al and large background coming from Ni. It is also intriguing that the TVA for the top-layer Al is strongly enhanced in the surface-normal direction while that for Ni is not very pronounced, as shown by our MEIS analysis and predicted by the present MD simulations. This is clearly explained by the fact that the top Al plane is expanded remarkably toward the vacuum side relative to the top Ni plane. Such a situation is also seen for nonpolar alkali-halide crystal surfaces such as RbI(001) and KI(001).[34,44]

VI. SUMMARY

The surface relaxation ($\Delta\varepsilon_{12}$) and rumpling of the top and second layers $[\Delta\varepsilon(1),\Delta\varepsilon(2)]$ are determined by high-resolution MEIS. The interlayer distance between the top and second layer ε_{12} is slightly expanded and the top Al plane is considerably displaced toward the vacuum side by 0.12 ± 0.02 Å above the Ni plane. Interestingly, the present MD and VASP calculations and XRD analysis give an expanded relaxation whereas the previous MEIS (Ref. 5) and MD (Ref. 28) and the other *ab initio* calculations[8,9] concluded contracted relaxation. Concerning the rumpling of the top layer, all the theoretical and experimental analyses result in considerable outward displacement of Al plane relative to the Ni plane. The present MEIS and MD simulations[29] give significant upward displacement of Ni plane relative to the Al plane in the second layer. However, the method to minimize the total energy based on the density functional theory is insensitive to the second-layer rumpling. We also determine the TVAs to be 0.10 ± 0.005 and 0.105 ± 0.01 Å, respectively, for the bulk Ni and for the top-layer Ni in the surface-normal direction. The former TVA agrees well with the value of 0.097 Å derived from the phonon-dispersion relation calculated using the VASP codes. The slightly enhanced TVA of the top-layer Ni in the surface-normal direction is compatible with the present MD simulations. As conclusion, the VASP codes as well as MD simulations using the EAM potentials are successfully applied to structure analysis and lattice dynamics of intermetallic binary alloy of NiAl. Indeed, they give reasonable values on the surface structure and lattice dynamics. So, both are probably applicable to any binary alloys, if the parameters for EAM potential in the MD simulations are adopted appropriately.

ACKNOWLEDGMENTS

The authors appreciate T. Nishimura for his help in carrying out the MEIS experiment. Thanks are also due to our colleagues, K. Mitsuhara, A. Iwamoto, Y. Kitsudo, and N. Isozaki for their assistant in the MEIS analysis. This work was partly supported by Japan Science and Technology Agency, JST, CREST.

*Corresponding author. FAX: +81-77-561-2657; ykido@se.ritsumei.ac.jp

[1] T. Okazawa, F. Takeuchi, and Y. Kido, Phys. Rev. B **72**, 075408 (2005).
[2] G. Kresse and J. Hafner, Phys. Rev. B **47**, 558 (1993).
[3] G. Kresse and J. Hafner, Phys. Rev. B **49**, 14251 (1994).
[4] H. L. Davis and J. R. Noonan, Phys. Rev. Lett. **54**, 566 (1985).
[5] S. M. Yalisove and W. R. Graham, Surf. Sci. **183**, 556 (1987).

[6] D. R. Mullins and S. H. Overbury, Surf. Sci. **199**, 141 (1988).
[7] X. Torrelles, F. Wendler, O. Bikondoa, H. Isern, W. Moritz, and G. R. Castro, Surf. Sci. **487**, 97 (2001).
[8] J. I. Lee, C. L. Fu, and A. J. Freeman, Phys. Rev. B **36**, 9318 (1987).
[9] A. T. Hanbicki, A. P. Baddorf, E. W. Plummer, B. Hammer, and M. Scheffler, Surf. Sci. **331-333**, 811 (1995).
[10] P. Rivière, H. F. Busnengo, and F. Martin, J. Chem. Phys. **121**, 751 (2004).
[11] J. R. Noonan and H. L. Davis, Science **234**, 310 (1986).
[12] R. M. Jaeger, H. Kuhlenbeck, H.-J. Freund, M. Wuttig, W. Hoffmann, R. Franchy, and H. Ibach, Surf. Sci. **259**, 235 (1991).
[13] A. Stierle, F. Renner, R. Streitel, H. Dosch, W. Drube, and B. C. Cowie, Science **303**, 1652 (2004).
[14] M. Schmid, M. Shishkin, G. Kresse, E. Napetschnig, P. Varga, M. Kulawik, N. Nilius, H.-P. Rust, and H.-J. Freund, Phys. Rev. Lett. **97**, 046101 (2006).
[15] T. Nishimura, Y. Hoshino, T. Okazawa, and Y. Kido, Phys. Rev. B **77**, 073405 (2008).
[16] S. Stempel, M. Bäumer, and H.-J. Freund, Surf. Sci. **402-404**, 424 (1998).
[17] S. Andersson, P. A. Brühwiler, A. Sandell, M. Frank, J. Libuda, A. Giertz, B. Brena, A. J. Maxwell, M. Bäumer, H.-J. Freund, and N. Mårtensson, Surf. Sci. **442**, L964 (1999).
[18] N. Nilius, N. Ernst, and H.-J. Freund, Phys. Rev. Lett. **84**, 3994 (2000).
[19] S. Lee, C. Fan, T. Wu, and S. L. Anderson, J. Chem. Phys. **109**, 381 (2005).
[20] Y. Kido, H. Namba, T. Nishimura, A. Ikeda, Y. Yan, and A. Yagishita, Nucl. Instrum. Methods Phys. Res. B **136-138**, 798 (1998).
[21] T. Nishimura, A. Ikeda, and Y. Kido, Rev. Sci. Instrum. **69**, 1671 (1998).
[22] Y. Kido and T. Okazawa, Surf. Rev. Lett. **10**, 389 (2003).
[23] P. L. Grande, A. Hentz, R. P. Pezzi, I. J. R. Baumvol, and G. Schiwietz, Nucl. Instrum. Methods Phys. Res. B **256**, 92 (2007).
[24] M. Hazama, Y. Kitsudo, T. Nishimura, Y. Hoshino, P. L. Grande, G. Schiwietz, and Y. Kido, Phys. Rev. B **78**, 193402 (2008).
[25] T. Okazawa, K. Shibuya, T. Nishimura, and Y. Kido, Nucl. Instrum. Methods Phys. Res. B **256**, 1 (2007).
[26] M. S. Daw and M. I. Baskes, Phys. Rev. B **29**, 6443 (1984).
[27] S. M. Foiles, M. I. Baskes, and M. S. Daw, Phys. Rev. B **33**, 7983 (1986).
[28] W. Kohn and L. J. Sham, Phys. Rev. **140**, A1133 (1965).
[29] S. Rubini and P. Ballone, Phys. Rev. B **48**, 99 (1993).
[30] Y. Mishin, M. J. Mehl, and D. A. Papaconstantopoulos, Phys. Rev. B **65**, 224114 (2002).
[31] E. Clementi and C. Roetti, At. Data Nucl. Data Tables **14**, 177 (1974).
[32] J. W. Otto, J. K. Vassiliou, and G. Frommeyer, J. Mater. Res. **12**, 3106 (1997).
[33] C. Kittel, *Introduction to Solid State Physics*, 4th ed. (John Wiley & Sons, New York, 1971).
[34] T. Okazawa, S. Ohno, Y. Hoshino, T. Nishimura, and Y. Kido, Nucl. Instrum. Methods Phys. Res. B **183**, 108 (2001).
[35] J. P. Perdew, K. Burke, and M. Ernzerhof, Phys. Rev. Lett. **77**, 3865 (1996).
[36] G. Kresse and D. Joubert, Phys. Rev. B **59**, 1758 (1999).
[37] G. Kresse and J. Furthmüller, Phys. Rev. B **54**, 11169 (1996).
[38] D. M. Bylander, L. Kleinman, and S. Lee, Phys. Rev. B **42**, 1394 (1990).
[39] M. Mostoller, R. M. Nicklow, D. M. Zehner, S.-C. Lui, J. M. Mundenar, and E. W. Plummer, Phys. Rev. B **40**, 2856 (1989).
[40] A. A. Maradudin, E. W. Montroll, G. H. Weiss, and I. P. Ipatova, *Theory of lattice dynamics in the harmonic aproximations*, in Solid State Physics Suppl. 3 (Academic Press, New York, 1971).
[41] K. Parlinski, Z. Q. Li, and Y. Kawazoe, Phys. Rev. Lett. **78**, 4063 (1997).
[42] J. Lindhard and M. Scharff, K. Dan. Vidensk. Selsk. Mat. Fys. Medd. **27**, 15 (1953).
[43] T. Okazawa, Y. Yagi, and Y. Kido, Phys. Rev. B **67**, 195406 (2003).
[44] T. Okazawa, T. Nishimura, and Y. Kido, Phys. Rev. B **66**, 125402 (2002).